Plasmonics (2020) 15:109–121
https://doi.org/10.1007/s11468-019-01014-8

Practical Implementation of Accurate Finite-Element Calculations for Electromagnetic Scattering by Nanoparticles

Johan Grand[1] · **Eric C. Le Ru**[1]

Received: 19 March 2019 / Accepted: 12 August 2019 / Published online: 23 August 2019

Abstract

The finite-element method (FEM) is increasingly used as a numerical tool to support experimental and theoretical studies of the optical properties of nanoparticles, in contexts such as surface-enhanced spectroscopy, molecular plasmonics, metamaterials, and optical trapping. Here, we investigate the validity of such calculations, focusing in particular on numerically challenging cases involving strong optical (plasmon) resonances and solutions with large electric field gradients and intensities. These are exemplified by elongated metallic nanoparticles and two closely spaced metallic spheres (dimer), where highly localized regions of intense electric field enhancements occur at the tip or in the gap, so-called electromagnetic hot-spots. We assess the accuracy of the FEM solutions by comparing the result to exact analytic solutions based on the T-matrix method for an elongated particle and generalized Mie theory for a dimer. Particular attention is given to the electromagnetic properties that have seldom been studied in this context, notably near-field properties such as surface-field enhancement factors and far-field radiation profiles. We also demonstrate explicitly how the accuracy of the FEM predictions can be inferred from the solution of two problems with different mesh and bounding box parameters. Such a numerical check is crucial in practice as no exact solutions are in general available to compare with. While we chose the commercial software COMSOL to illustrate our results, the methods and conclusions are equally applicable to other FEM implementations. We provide for convenience full details of how to set up these calculations in COMSOL, which we hope will allow readers to easily reproduce them and seamlessly adapt them to their modeling needs. We expect this work will cement the FEM as a reliable method for routine calculation of electromagnetic scattering by nanoparticles.

Keywords Localized surface plasmon resonance · Finite-element method · T-matrix · Generalized Mie theory · Nanoparticles

Introduction

Efficient and accurate numerical solutions of Maxwell's equation form an integral part of many research endeavors [1–4]. For example, in the context of electromagnetic (EM) scattering by particles, numerical solutions can be used to calculate the scattering properties of aerosol for climate research [5], or of interstellar dust in astrophysics [1, 6], the near fields in the context of surface-enhanced spectroscopy [7, 8], or for optical tweezing [9]. While analytic or semi-analytic solutions such as Mie theory [10] or the T-matrix method [11] are ideal, their range of applicability can be limited to specific types of scatterers. Fully numerical partial differential equation solvers such as finite-difference time domain (FDTD) [12] and the finite element method (FEM) [13, 14] provide the most general solution and are typically applicable to any particle shapes, groups of particles, and particles on a substrate. Their main disadvantages are the computing resources required (time and memory) and the accuracy of the obtained solution, which is intimately linked to the computing resources invested. The latter aspect is particularly problematic as there is no systematic easy method to assess the accuracy of the obtained solution, except by comparing it with a

Electronic Supplementary Material The online version of this article (https://doi.org/10.1007/s11468-019-01014-8) contains supplementary material, which is available to authorized users.

✉ Johan Grand
johan.grand@univ-paris-diderot.fr

[1] The MacDiarmid Institute for Advanced Materials and Nanotechnology, School of Chemical and Physical Sciences, Victoria University of Wellington, PO Box 600, Wellington, 6140, New Zealand

known solution. In a typical FDTD or FEM electromagnetic scattering problem, the accuracy of the numerical solution will notably depend on:

- The finesse of the discretization of space (i.e., of the mesh)
- Bounding box effects, in particular, its size (i.e., how far it is from the scatterers) and the chosen boundary conditions, which are typically chosen to minimize back-reflection of the scattered field
- For iterative solutions (which remains typically the case for large 3D simulations), the choice of numerical solver and, possibly, pre-conditioner

The development of perfectly matched layers (PMLs) for the bounding box [13–15] has allowed significant progress in the overall accuracy of FEM for EM scattering. Even then, the effect of PMLs on the accuracy of FEM simulations remains strongly dependent on several factors: how far they are from the scatterer, how thick the PMLs are, and how finely they are meshed. There have been a few attempts to quantify the accuracy of FEM for electromagnetic scattering by nanoparticles (NPs) [3, 16–23] by comparing it either to analytic/semi-analytic solutions or to other numerical methods. Some of these studies have also compared different implementations (software) of the FEM [16, 23], including COMSOL, JCMsuite, HFSS, and CST Microwave Studio. In most cases, these comparisons have been limited to simple configurations, primarily spheres [3, 20–22] or spherical nanoshells [17], although spheroids [19], nanocubes [23], and dimers of interacting spheres [16] and nanoshells [18] have also been considered. The vast majority of these studies are rather shy on the details of the practical implementation of the calculations. Even when details are provided, the influence of the choice of parameters is rarely studied or even discussed. This leaves prospective users with little insight into how to set up their own calculations. The accuracy of FEM calculations is so dependent on the parameters discussed above that it is not possible to extrapolate results for one type of nanoparticle to another, or from far-field accuracy to near-field accuracy, etc. Especially since the expertise/know-how of the user can play a big part in the accuracy obtained. For example, Ref. [16] concluded that software *X* had the worst accuracy and later corrected that claim after someone pointed out how a comparable accuracy could be obtained with proper use of software *X* features. Despite these uncertainties, FEM calculations are now increasingly used without further justification, in challenging situations such as elongated/pointy particles or interacting nanoparticles with small $\sim$ nm gaps where large electric field enhancements and strong plasmon resonances occur, which may inflate any bounding box issues in a non-predictable way.

In this work, we carefully assess the validity of such calculations by comparing them to semi-analytic results of high accuracy: T-matrix theory for elongated particles (prolate spheroids) [24], and generalized Mie theory for dimers [25]. We consider relevant EM quantities in both the near field, such as surface-field enhancements and far-field, such as radiation profile. We pay particular attention to the practical implementation of those FEM calculations in COMSOL, with comprehensive descriptions and Supplementary Material to allow readers to reproduce our simulations themselves. COMSOL, moreover, enables the user to solve interdependent physics problems within the same domain, which means that those models can readily be extended to study, for example, nanoparticle heating and other multiphysics problems [21]. We believe this work will cement the validity of FEM for EM scattering of nanoparticles and serve as a benchmark for future FEM calculations in the context of plasmonics and nanophotonics.

General Considerations

In this work, we will consider the standard problem of EM scattering by a particle [11]. We use complex notations for the electromagnetic fields with a time dependence chosen as $\exp(+i\omega t)$. This is different from the commonly used convention in physics but is prevalent in engineering and is the one chosen in COMSOL, which we use for all our example calculations. The particle is embedded in a non-absorbing medium of relative dielectric function ϵ_1 and excited at a wavelength λ by an incident field $\mathbf{E}_{\text{inc}}(\mathbf{r})$ consisting of a plane wave of amplitude E_0 incident along z and polarized along x. The wavevector is denoted $k_1 = (2\pi/\lambda)\sqrt{\epsilon_1}$ and we therefore have $\mathbf{E}_{\text{inc}}(\mathbf{r}) = E_0\mathbf{e}_x \exp(-ik_1 z)$. As customary, the solution can be written as $\mathbf{E}(\mathbf{r}) = \mathbf{E}_{\text{inc}}(\mathbf{r}) + \mathbf{E}_{\text{sca}}(\mathbf{r})$ where $\mathbf{E}_{\text{sca}}(\mathbf{r})$ denotes the scattered field. To compare the performance of our FEM calculations, we will calculate several derived EM properties listed below. For maximum generality, we include in those both far-field and near-field properties, along with quantities that can be calculated with alternative methods to check the self-consistency of the results.

- The scattering cross section is calculated by integrating the flux of the complex Poynting vector of the scattered field, $\mathbf{S}_{\text{sca}}$, across the nanoparticle surface:

$$\sigma_{\text{sca}} = \frac{1}{S_0} \iint_{\text{NP}} \text{Re}\left(\mathbf{S}_{\text{sca}}(\mathbf{r}) \cdot \mathbf{n}\right) dS,$$

where $S_0 = \frac{\sqrt{\epsilon_1} E_0^2}{2Z_0}$ is the power density of the incident field and $Z_0 = \sqrt{\frac{\mu_0}{\epsilon_0}} \approx 376.73\ \Omega$ is the characteristic impedance of vacuum.

- The absorption cross section is calculated from a volume integral inside the NP:

$$\sigma_{\text{abs}} = \frac{1}{S_0} \iiint_{\text{NP}} Q_h \, dV,$$

where $Q_h = \frac{1}{2}\omega\epsilon_0 \text{Im}(\epsilon_2(\omega))|\mathbf{E}(\mathbf{r})|^2$ is the total power dissipation density. $\epsilon_2(\omega)$ denotes the relative dielectric function of the particle (possibly complex and wavelength-dependent).

- The extinction cross section is then simply calculated from energy conservation as

$$\sigma_{\text{ext}} = \sigma_{\text{abs}} + \sigma_{\text{sca}}.$$

- We also calculate the radiation profile in order to more carefully assess the accuracy of the far-field calculations in FEM and in particular the COMSOL far-field module. To this end, the scattering amplitude, denoted E_{far}, is defined as:

$$\mathbf{E}_{\text{sca}}(\boldsymbol{r}) = \frac{\exp(-ik_1 r)}{r}\mathbf{E}_{\text{far}}(\theta, \phi).$$

Note that different conventions may be used here, so we chose the one closest to COMSOL's far-field implementation (see discussion in Appendix for details). It should be noted that $\mathbf{E}_{\text{far}}(\theta, \phi)$ is not directly calculated in the FEM model because of the finite nature of the bounding box. It can, however, be derived from the near fields (for example, the fields on the surface of the particle) using a formalism similar to the Stratton-Chu formula [27, 28]. For convenience, this post-processing step is implemented in COMSOL. As the COMSOL documentation on the subject is somewhat incomplete, we summarize all the required formulae for far-field calculations in the Appendix. We will look in particular at the scattering matrix elements S_1 and S_2.

- From the scattering amplitudes, it is possible to also calculate the extinction cross section from the optical theorem [10, 11], to check the self-consistency of the solution. The optical theorem relates the extinction cross section to the scattering amplitude evaluated in the forward direction ($\theta = 0$) along the incident polarization. With our conventions and notations, this takes the following form:

$$\sigma_{\text{ext}}^{\text{OT}} = \frac{-4\pi}{k_1 E_0}\text{Im}\left\{\mathbf{E}_{\text{far}}(\theta = 0) \cdot \mathbf{e}_x\right\}.$$

- One important characteristic of EM scattering applied to plasmonics is the intensity of the largest field enhancement on the NP surface and how strongly localized it is. These are important properties, for example, in the context of surface-enhanced Raman spectroscopy hot-spots [7]. Large field intensities and the associated large field gradients are also expected to be the most challenging aspects of any numerical calculations, and it is therefore crucial to specifically quantify the accuracy in such cases. To this end, we will compute the local field intensity enhancement factor [8]:

$$M(\mathbf{r}) = \left|\frac{\mathbf{E}(\mathbf{r})}{E_0}\right|^2.$$

As this is position-dependent, we will focus on calculations at a single wavelength, typically close to the plasmon resonance maximum λ_R and study the variation of $M(\mathbf{r})$ along an arc length on the NP surface, where the maximum fields and largest gradients are expected. Alternatively, the variation along a cutline across the bounding box and NP will also give an indication of the accuracy of the solution inside the NP and as a function of distance from it.

- In order to capture the wavelength dependence of near-field properties, we will also consider the surface-averaged local field intensity enhancement factor:

$$\langle M \rangle = \frac{1}{A}\iint_{\text{NP}} \left|\frac{\mathbf{E}(\mathbf{r})}{E_0}\right|^2 dS,$$

where A is the surface area of the particle and $\mathbf{E}$ is the surface field (outside the NP). The advantage of this single quantity is that it can easily be plotted against wavelength to characterize the plasmon resonance in the near field.

While the scattering, absorption, and extinction cross-sections have been commonly used in studies of the performance of FEM calculations, the other properties discussed above have only been considered in isolated cases. For convenience, explicit formulae and details on how all these properties are calculated in COMSOL are given in the Appendix.

For all the quantities considered, we will calculate the relative error e between the FEM predictions A_{FEM} and the exact numerical results A_{ex}, explicitly $e = |1 - A_{\text{FEM}}/A_{\text{ex}}|$. When the quantity is position or wavelength-dependent, we may also compute its RMS value $\sqrt{\langle e^2 \rangle}$ (where $\langle\rangle$ denotes the average value) to quantify with a single number the accuracy.

Finally, we note that for highly symmetric structures such as those considered in this work, it is possible to exploit symmetries to reduce the meshed domain, typically to one-quarter of the space. This can dramatically reduce the memory requirements and speed up the computations. Because we aim to show that accurate FEM calculations can be routinely carried out on particles of arbitrary shapes, we will deliberately not exploit these symmetries. Our FEM models can, therefore, be directly adapted to arbitrary particle shapes.

Single Gold Spherical Particle

We first consider a spherical particle as Mie theory provides a reliable analytical solution to the electromagnetic scattering by a sphere [10] and it is an important system in many types of experiments [29–31]. This simple system has previously been used as a benchmark for FEM/COMSOL, but often in situations where the plasmon resonance was strongly damped, typically for a gold sphere in vacuum [3, 20]. For completeness, we therefore revisit it here and include in addition a discussion of the calculations of the radiation profile (far-field) and the effect of PML meshing. Calculations were run for a single gold spherical NP surrounded by a homogeneous non-dispersive medium of $\epsilon_1 = 4$. This dielectric constant was chosen to push the NP resonance to ~ 650 nm where the optical absorption of gold is relatively low and comparable with that of silver. The electromagnetic fields will thus be more intense and the gradient/bounding box effects more challenging. The diameter of the sphere is taken as 60 nm. The dielectric function of gold used in the simulations is the analytical expression derived in [32]. The results are compared with Mie theory as implemented in the SPlaC package [8, 33] for which high precision results are obtained for both far-field and near-field properties [26]. The detailed implementation of this model in COMSOL is provided in the Appendix. A critical ingredient is the use of a PML condition for the bounding box. PMLs consist of an outer layer made of a virtual material with specific complex-valued anisotropic permittivity and permeability, which can be cumbersome to define manually. COMSOL provides a ready-for-use implementation of PMLs in standard geometries, namely, for spherical, cylindrical, or cuboid bounding boxes. It remains the user's responsibility to correctly choose the PML shape and thickness and to apply a suitable mesh. It is sometimes stated that at least five mesh elements are needed across the thickness of the PML for it to fulfil its purpose (which we recall is absorbing all the outgoing waves). This is checked explicitly in Fig. 1. It is clear from those results that the correct meshing of the PML region is critical for the accuracy of the simulation. By default, COMSOL will mesh this region with only one mesh layer, which results in reduced accuracy for all optical properties. Special tools (swept or mapped meshes) must be applied to force the mesh to include more layers (as detailed in the Appendix) and recover a better accuracy. The thickness of the PML (100 nm in Fig. 1) was not found to affect the accuracy significantly when either increased to 500 nm or decreased to 50 nm (not shown here). The location of the PML inner layer was set at 250 nm from the center of the NP (i.e., outer PML at 350 nm). It is usually

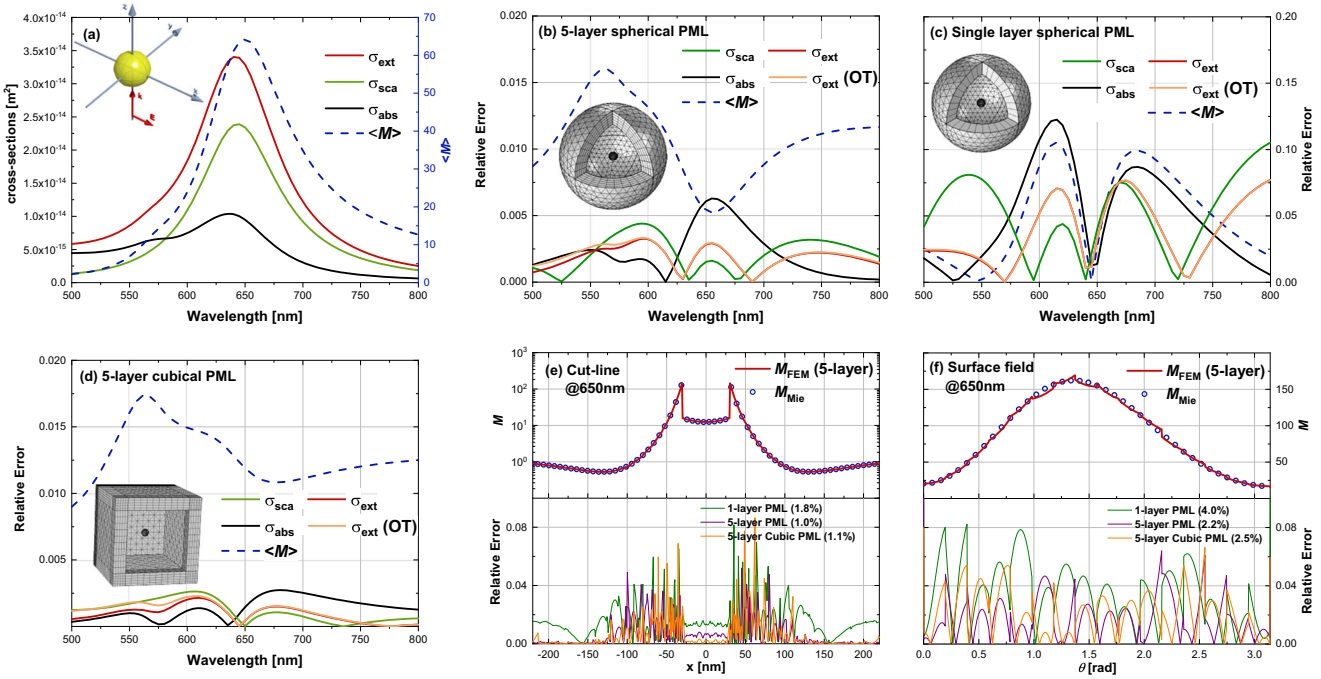

Fig. 1 Accuracy of the FEM for a 60-nm diameter gold sphere embedded in a medium with $\epsilon_1 = 4$, against Mie theory results for which the relative accuracy is of the order of 10^{-14} [26]. **a** Wavelength dependence of the extinction, scattering, and absorption cross sections and surface-average EF (all from Mie theory). **b–d** Relative errors in the same EM properties, as calculated from FEM with spherical PMLs meshed with either 5 **b** or 1 **c** layer and with cubical PMLs meshed with 5 layers **d**. **e** Position-dependent EF, $M(x)$, on a cutline along x across the bounding box (top panel), along with the relative error (bottom panel) from the same FEM solutions as in **b–d**. These are computed for $\lambda = 650$ nm, i.e., close to the plasmon resonance of the sphere. **f** Same as **e** but for the position-dependent EF, $M(\theta)$, on the NP surface (outside) in the cut plane xOz. The RMS error for each PML configuration is specified in the legend of the bottom panels of **e** and **f**

recommended to be at least 2–3 times, the maximum scatterer dimensions and it did not appear to be a limiting factor in the accuracy of our calculations (see also the discussion in "Self-Referencing Accuracy Assessment"). We also compare in Fig. 1 the results for two PML shapes, spherical and cubical of comparable dimensions. The far-field cross sections appear more accurate with the cubical PML, but it is not clear why this occurs, as the local field errors remain comparable. In any case, the larger volume and surface area of the PML region for a cubic box results in an increase in the number of mesh elements and a corresponding increase in computing time by a factor of ~ 3. The spherical PML is also arguably easier to set up. For these reasons, we will therefore use the spherical PML in the following.

Another often overlooked aspect in previous studies of the applicability of the FEM is the accuracy of the far-field scattering amplitudes or radiation profile. In a recent study, Yang et al. [22] have developed a method to retrieve this information from the near-field solution in the most general case, notably in the presence of a substrate or a waveguide. For scattering by a bounded object, as considered in this work, a much simpler approach based on the Stratton-Chu formula [27, 28] can be used. This method is implemented in the built-in far-field module of COMSOL, and the definitions of the quantities calculated in this module are summarized in the Appendix for convenience. The accuracy of the computed radiation profiles (at resonance, $\lambda = 650\,\text{nm}$) is studied in Fig. 2. As for other properties, an acceptable relative error is obtained but this error can vary significantly depending on the quality of the PML region. For example, the error is ~ 4 times larger for a 1-layer PML compared with the 5-layer PML, reinforcing the importance of including multiple mesh layers in the PML. COMSOL also allows the user to choose the surface of integration for far-field computations. In most simulations, the particle surface has a finer mesh than the region surrounding it, and is therefore the natural choice for the implementation of Stratton-Chu formula. As shown in Fig. 2, choosing instead the bounding box surface results in a significant degradation in the far-field predictions.

Overall, with the 5-layer spherical PML and the parameters summarized in Table 1, a relative error of less then 1% is achieved in all computed cross sections, and less than 5% in all field EF (surface fields or along cutlines). In many instances, the accuracy is in fact much better than these maximum values.

Single Silver Prolate Particles and Spherical Gold Dimer

While the spherical geometry is convenient thanks to the relative ease with which the results can be compared with exact

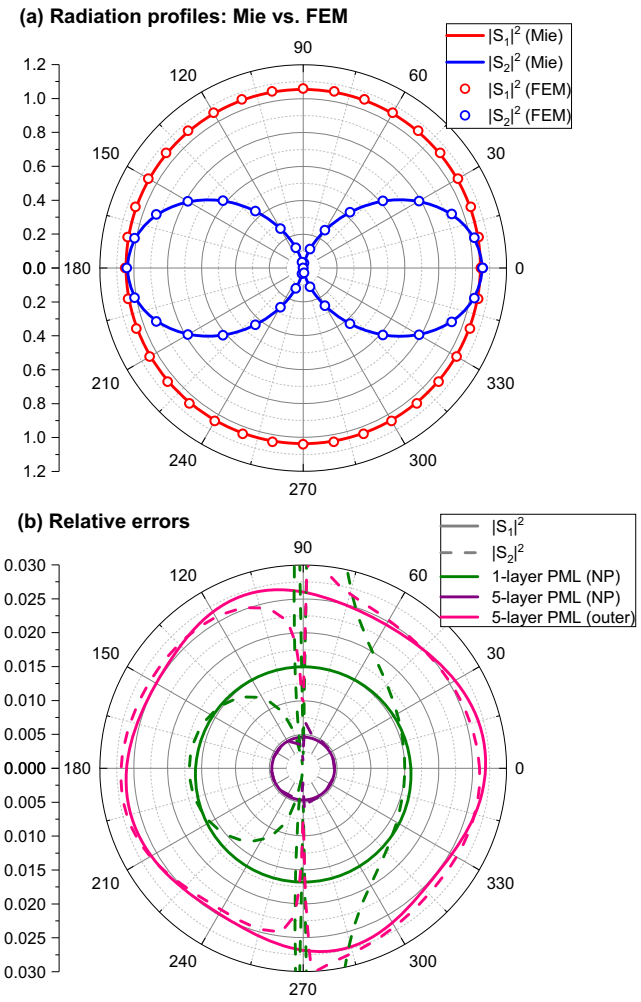

Fig. 2 Accuracy of the Stratton-Chu near-field to far-field transformation using the built-in COMSOL far-field module, as compared with the exact results of Mie theory. **a** The radiation profiles are represented as polar plots of $|S_1(\theta)|^2$ and $|S_2(\theta)|^2$ (see definitions in the Appendix) in solid lines for Mie theory and circles for the FEM simulations. A spherical PML with 5 meshed layers was used for the simulations. **b** Relative errors of the same far-field properties with spherical PMLs meshed with either 5 or 1 layers. For the 5-layer PMLs, the surface of integration was chosen to be either the NP (purple lines) or the bounding box surface (pink lines)

solutions from Mie theory, it is not representative of the general geometries relevant to experimental nanophotonics, which may notably involve elongated/pointy particles [34–36] or/and closely interacting NPs [37–39]. In those cases, new problems may arise due to the lower symmetry of the problem: stronger resonances are typically exhibited, associated with large field enhancements and gradients, especially close to tips or narrow gaps. We will, therefore, assess those situations, starting with elongated particles for which the T-matrix method provides accurate semi-analytical results [11]. In particular, we will use a formulation we recently developed for spheroidal particles [40, 41], for which the high accuracy of the solution can be

Table 1 Summary of the simulation parameters. DOF refers to the total number of degree of freedom

Geometry	DOF	Mesh elements on NP sfce	PML				RMS errors (%)	
			Type	Inner length	Thickness (nm)[a]	# layers (nm)	σ_{ext}	$\langle M \rangle$
Sphere	1 131 452	852	Cubical	250	100	5	0.11	1.30
Sphere	599 078	852	Spherical	250	100	5	0.20	1.11
Sphere	524 026	852	Spherical	250	100	1	4.58	6.07
"Fine Mesh"								
Prolate #A	889 520	3268	Spherical	250	100	5	0.21	0.47
Prolate #B	1 558 490	5752	Spherical	290	60	5	–	–
Sphere-dimer #A	1 061 850	7398	Spherical	250	100	5	0.17	0.19
Sphere-dimer #B	1 510 992	9264	Spherical	290	60	5	–	–
"Coarse Mesh"[b]								
Sphere-dimer #A	204 926	1510	Spherical	250	100	5	14.6	15.9
Sphere-dimer #B	280 972	1916	Spherical	290	60	5	–	–

The number of mesh elements on the NP surface is set first and is one of the most crucial parameters. It indirectly affects the meshing inside and outside the particle as the mesh grows. In all situations the outside bounding box dimensions were set at 350 nm (increasing it did not improve the accuracy in our tests). Changing the PML thickness therefore affects the inner PML boundary location

[a]Distance from the center of the NP to the PML boundary

[b]A direct solver has to be used for the coarse mesh calculation, as an iterative one is likely not to converge for such a poor meshing. Conversely, an iterative solver is required for the fine mesh set up, as a direct matrix inversion would require too much computer memory

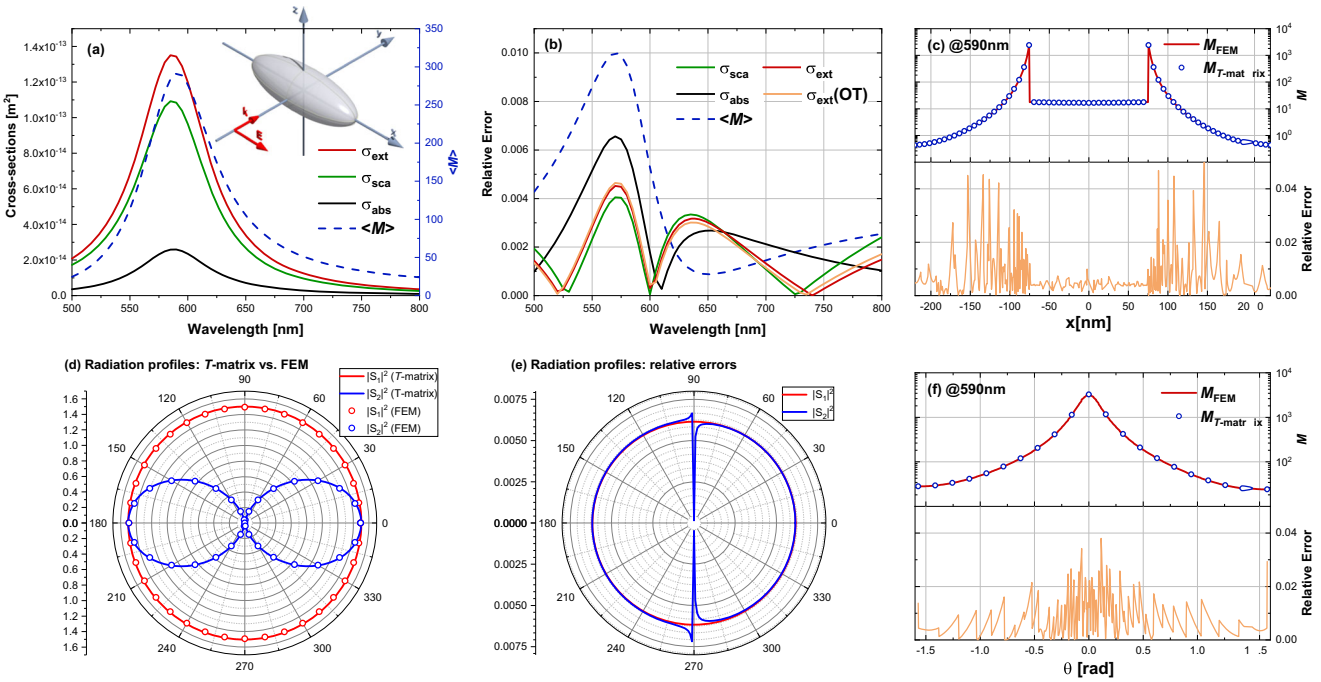

Fig. 3 Accuracy of the FEM for a 50:150 nm silver prolate particle in air, against T-matrix results. **a** Wavelength dependence of the extinction, scattering, and absorption cross sections and surface-average EF (all from T-matrix theory). **b** Relative errors in the same EM properties, as calculated from FEM with a 5-layer spherical PML. **c** Position-dependent EF, $M(x)$, on a cutline along x across the NP long axis and bounding box (top panel), along with the relative error (bottom panel). The cutline is computed at $\lambda = 590$ nm, i.e., close to the plasmon resonance along the NP long axis. **d**, **e** Radiation profiles of the prolate NP, represented as polar plots of $|S_1(\theta)|^2$ and $|S_2(\theta)|^2$ (see definitions in the Appendix) calculated using the far-field module of COMSOL (solid lines) and the T-matrix theory (circles). **e** Relative error for these two elements of the scattering amplitude matrix. **f** Same as **c** but for the position-dependent EF, $M(\theta)$, on the NP surface (outside) in the cut plane xOz

explicitly quantified [24], including for near-field properties [28]. The codes are also freely available [42]. We consider a silver prolate particle in air with an aspect ratio of 1:3 and dimensions 50 × 150 nm. The PML is taken as 5-layer spherical; the k-vector of the incident EM field is set perpendicular to the long axis and the polarization parallel to it. We calculate the different cross sections (absorption, scattering, and extinction, see Fig. 3a), the average EF along the NP long axis (Fig. 3c), and the average EF just outside the NP surface in the cut plane xOz (Fig. 3f). The cutlines were computed at the main plasmon resonance wavelength, namely 590 nm. The scattering amplitude matrix elements $|S_1|^2$ and $|S_2|^2$ are also plotted in Fig. 3d and e. The relative errors (against T-matrix method results) of all those quantities are also shown in Fig. 3. Similar conclusions to those obtained for the sphere can be drawn from this figure with relative errors of less than 1% for cross sections, and less than 5% for fields.

Another commonly encountered plasmonic system is the dimer of nanospheres, for which generalized Mie theory (GMT) conveniently provides analytical solutions [7, 25]. We consider two 60-nm gold NP in water ($\epsilon_1 = 1.77$), separated by 1 nm. The k-vector of the incident light is set perpendicular to the long axis of the dimer, and the polarization parallel to it. Under these conditions, a high EM field and associated large gradients are expected in the region of the gap between the NPs, making the convergence of the calculations more challenging than in the case of isolated NP [16]. The results of FEM calculations and their error relative to GMT are summarized in Fig. 4. The EM-field confinement can be observed in Fig. 4 where the average EF is plotted on a line across the gap (d) and on

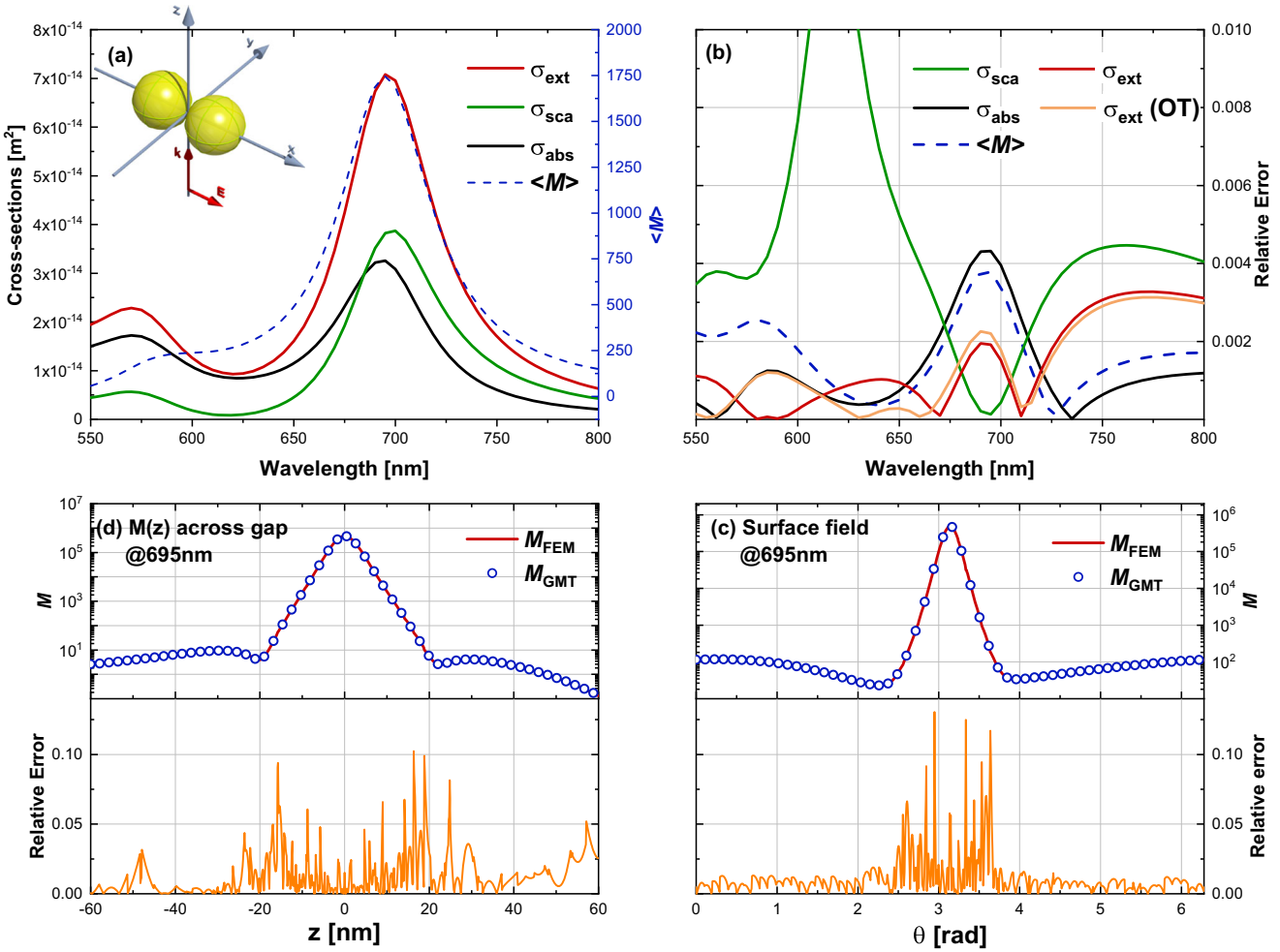

Fig. 4 Accuracy of the FEM for a dimer consisting of two 60-nm gold spheres separated by a 1 nm gap in water ($\epsilon_1 = 1.77$), against GMT results. **a** Wavelength dependence of the extinction, scattering, and absorption cross sections and surface-average EF (all from GMT). **b** Relative errors in the same EM properties, as calculated from FEM with spherical PMLs meshed with 5 layers. **c** Position-dependent EF at $\lambda = 695$ nm, $M(x)$, on a cutline along x across the bounding box (top panel), along with the relative error (bottom panel). **d** Same as **c** but for the position-dependent EF (top panel), $M(\theta)$, on the NP surface (outside) in the cut plane xOz, and the corresponding relative error (bottom panel)

the outer surface of one of the NP (c). The large field intensity enhancement of almost 10^6 in the gap at resonance is correctly predicted (within 3%) by FEM. The surface field in the gap region is predicted with a larger relative error of 10%. As before, all cross sections are correct to within 1%, except for the scattering cross section around 600 nm. In this case, the cross section is, in fact, close to zero, thereby pushing up artificially the relative error, but the absolute error remains small.

Self-Referencing Accuracy Assessment

For all the cases studied so far, the FEM outputs were compared with the exact solution of the EM problem provided either by Mie theory, GMT, or the T-matrix method. We were then able to assess the impact of different key input parameters like the mesh or the PML geometry on the simulation accuracy. But can we estimate the accuracy of a numerical simulation when no exact solution of the problem is readily available? The most obvious approach would be to refine the mesh repeatedly and ensure that the results have converged. However, any mesh refinement typically increases significantly the number of degrees of freedom and, therefore, the memory requirements and computing time, in many cases beyond what is practical. Moreover, refining the mesh will not detect any problems associated with the influence of the bounding box, which should be checked by increasing the bounding box size. We hereby instead propose a method to obtain an error estimate for the predicted quantities by comparing results from two FEM simulations ran with slightly different mesh parameters and/or different bounding box sizes. The aim is not to use the second simulation to improve the predictions but to

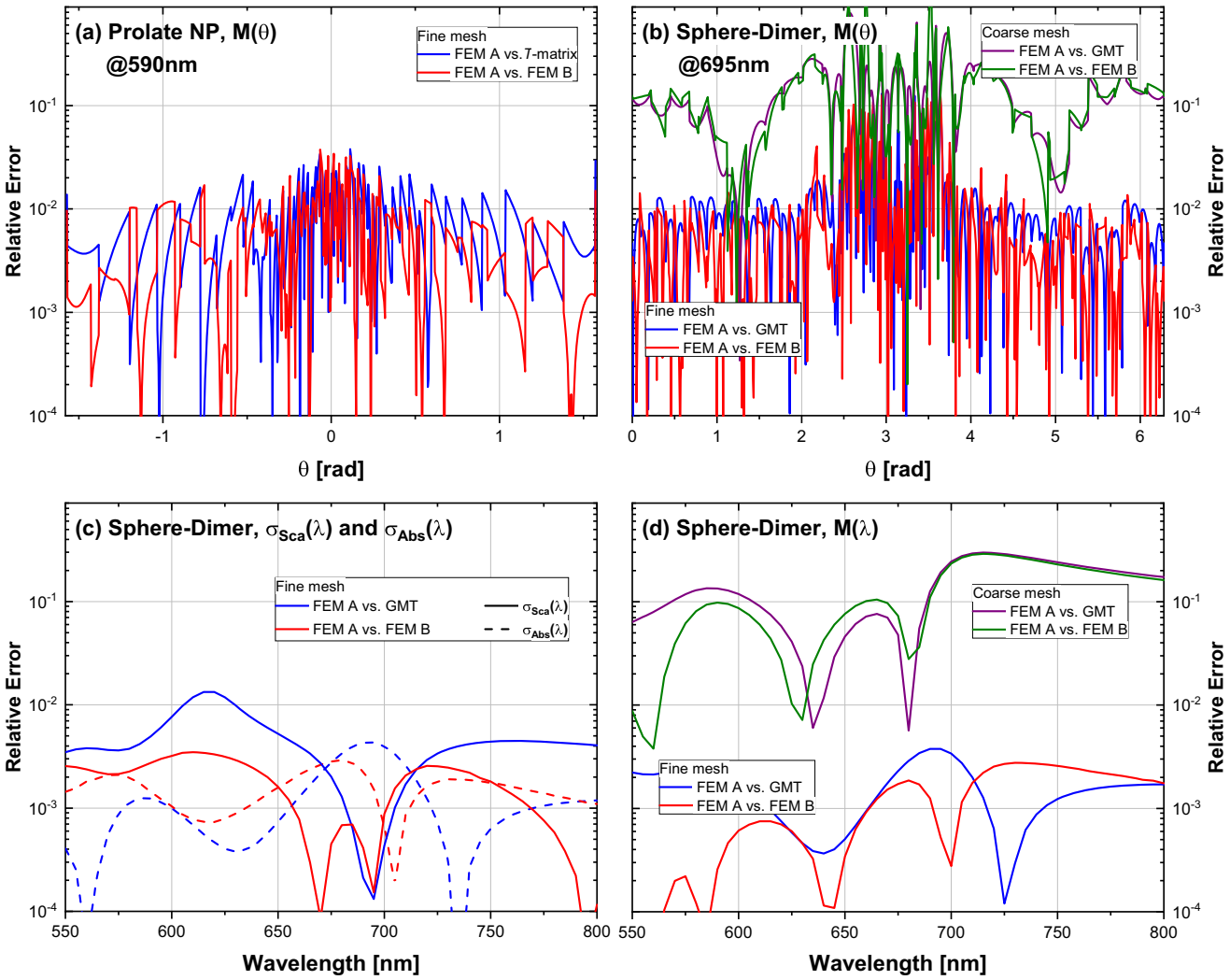

Fig. 5 Relative errors obtained by comparing the FEM predictions from two simulations with different parameters for the mesh and the bounding box size (runs A and B in Table 1. These are compared with the relative errors with respect to the exact solution (T-matrix for the spheroid NP, GMT for the NP-dimer). In the NP-dimer case, we show explicitly how the mesh finesse affects the FEM errors and how the FEM A vs FEM B comparison provides a good predictor of the relative error, which does not require a knowledge of the exact solution

obtain predictions with a comparable accuracy but a different error. A comparison between the two predictions then gives an estimate of the error, $e = |1 - A_{\mathrm{FEM\,A}}/A_{\mathrm{FEM\,B}}|$. This approach is illustrated in Fig. 5 in the cases of the spheroid NP and dimer studied earlier. The simulations are run twice with different sets of parameters (A and B), as summarized in Table 1. The meshing parameters are changed slightly to obtain a different mesh (not necessarily much finer). Similarly, the bounding box and PML parameters are slightly modified to avoid a systematic error associated with the influence of the bounding box in both simulations. As shown in Fig. 5, the relative error between run A and B is of comparable magnitude as the relative error in the predictions of either A or B (compared with the exact results). This is shown explicitly for the dimer in (b) and (d) by changing significantly the mesh finesse to induce a large change in the error in the FEM predictions (coarse mesh vs fine mesh), see also Table 1. The predictor based on FEM A vs FEM B then tracks closely the real error in each case, which we can here quantify by comparing with the exact results. This suggests that this predictor can be used to quantify the error in practical situations where no exact results are available.

Conclusion

These results demonstrate that accurate electromagnetic predictions of systems relevant to nanophotonics, with acceptable relative errors of the order of less than 1% for far-field properties and less than 5% to 10% for near-field, can now be achieved routinely with FEM calculations on standard computers. These include challenging cases such as computing the near fields of elongated nanoparticles or in small gaps between nanostructures. Special care must nonetheless be taken to set up the bounding box with a suitable PMLs and ensure the mesh is sufficiently fine. For any numerical calculations, it is paramount that the error in the predictions be reliably quantified. For this, we proposed and demonstrated a simple approach based on running the same simulation with two sets of parameters. We hope this work will cement the FEM as a reliable method for the calculation of the optical properties of nanoparticles.

Appendix A: Additional Details for the Practical Implementation in COMSOL

One example of COMSOL report file is provided as a Supplementary Material for the 60-nm diameter gold sphere embedded in a medium with $\epsilon_1 = 4$ simulation. It contains the full details of the simulations set up and should allow other COMSOL user to rerun the very same simulations.

A.1 General Comments

In the following, we assume the user is already familiar with COMSOL and only highlight a number of important comments/tips/clarifications for setting up this simulation, along with common traps/mistakes:

- All simulations were set up using the "Electromagnetic Waves, Frequency Domain (emw)" node of COMSOL 5.3 (which is part for example of the wave optics or radio frequency modules). This mode solves for the complex electric field, which is a vector quantity denoted `Ex, Ey, Ez`. Most other predefined quantities in the model are called as `emw.variablename` and can be seen in the `emw` node provided that the option "equation view" has been selected in the "Model Builder" window. Additional variables can be defined by the user prior to the computation.
- For convenience, we define a new parameter in the "Global Definitions" of the model builder called `lambda` corresponding to the wavelength in nm. Wavelength dependence is then carried out as a parametric sweep on `lambda`.
- It should be noted that COMSOL uses the engineer convention for the definition of the complex fields, i.e., with a factor $\exp(+i\omega t)$ for the time dependence; hence, the imaginary part of the dielectric function is negative for passive materials. In practice, ϵ is simply the complex-conjugate of what it would be with the $\exp(-i\omega t)$ convention more commonly used in physics. For example, the relative dielectric function of gold is obtained from the analytic expression of Ref. [32] as:

```
conj(1.54*(1-1/(177.5^2*((1/lambda)^2
+i/(14500*lambda))))
+1.27/470*(exp(i*(-pi/4))/(1/470-1/lambda
-i/1900)+exp(-i*(-pi/4))/(1/470+1/lambda
+i/1900))+1.1/325*(exp(i*(-pi/4))/(1/325
-1/lambda-i/1060)+exp(-i*(-pi/4))/(1/325
+1/lambda+i/1060)))
```

- The variable `epsilon1` is defined in the global definitions and is the relative dielectric constant, ϵ_1, of the external/surrounding medium.
- In order to implement PMLs on the bounding box, it is important to solve the problem for "scattered field", i.e., for $\mathbf{E}_{\mathrm{sca}}$ as opposed to solving directly for the total field $\mathbf{E} = \mathbf{E}_{\mathrm{sca}} + \mathbf{E}_{\mathrm{inc}}$. This option is specified in the "physics" (emw) node. We will only consider plane waves for the incident field $\mathbf{E}_{\mathrm{inc}}$ (called "background electric field" in the `emw` node). This is set

as $E_0\ \exp(-ik_1 z)\mathbf{e}_x$ (i.e., x-polarized and propagating along $+z$) with $k_1 = k_0\sqrt{\epsilon_1}$.

A.2 Computation of Electromagnetic Properties in COMSOL

The electromagnetic (EM) properties considered in this work are defined in the main text. In COMSOL, they can be computed by defining new "variables" as described below.

- For convenience, we first define several commonly used integrals as "components couplings" in the "definitions" node of COMSOL.

  `int_surf`: surface (double) integral on the NP surface.

  `int_vol`: volume (triple) integral inside the NP.

  `int_OT`: this is defined as an integral over a point located in the forward scattering direction and therefore is not *per se* an integral, but just a convenient way of evaluating the forward scattering amplitude to calculate the extinction cross section with the optical theorem (see below).
- The scattering cross section is calculated by integrating the flux of the complex Poynting vector of the scattered field $\mathbf{S}_{\text{sca}}$ across the nanoparticle surface:

$$\sigma_{\text{sca}} = \frac{1}{S_0}\iint_{\text{NP}} \text{Re}\left(\mathbf{S}_{\text{sca}}\cdot\mathbf{n}\right)\, dS,$$

  where $S_0 = \frac{E_0^2}{2Z_1}$ is the power density of the incident field and $Z_1 = Z_0/\sqrt{\epsilon_1}$ with $Z_0 = \mu_0 c = \approx 376.73\ \Omega$ the characteristic impedance of vacuum. E_0 is chosen arbitrarily as 1 V/m in all the simulation, but by linearity the results do not depend on this choice. For this we therefore define the following parameters:

```
E0 = 1 [V/m]
Z1 = Z0_const / sqrt(epsilon1)
S0 = E0^2 / (2*Z1)
```

And the variables:

```
nrelPoav=nx*up(emw.relPoavx)
         +ny*up(emw.relPoavy)
         +nz*up(emw.relPoavz)
sigma_sc = int_surf(nrelPoav)/S0
```

- The absorption cross section is calculated from the volume integral of the total power dissipation density inside the NP:

$$\sigma_{\text{abs}} = \frac{1}{S_0}\iiint_{\text{NP}} Q_h\, dV.$$

  In COMSOL, this gives:

```
sigma_abs = int_vol(emw.Qh)/S0
```

- The extinction cross section is calculated in two ways, either from energy conservation or from the optical theorem (OT):

```
k1 = emw.k0 * sqrt(epsilon1)
sigma_ext = sigma_sc+sigma_abs
sigma_extOT = -4*pi/k1
        *int_OT(imag(emw.Efarx*1[m]))/E0
```

- The surface-averaged local field intensity enhancement factor is obtained from

$$\langle M\rangle = \frac{1}{A}\iint_{\text{NP}} \left|\frac{\mathbf{E}(\mathbf{r})}{E_0}\right|^2 dS$$

  where A is the surface area of the particle and $\mathbf{E}$ is the surface field (outside the NP). Explicitly:

```
sigma_geom = int_surf(1)
M_ave = int_surf((up(emw.normE))^2)
                        /sigma_geom
```

It is important to point out that for surface integrals of non-continuous quantities (like the electric field across the NP surface),COMSOL will by default take the average value of the outside and inside integrand. This is clearly not what we want, so we need to specify that we choose the norm of the electric field on only one side of the surface. Every surface in COMSOL has two opposite intrinsic normal unit vectors defined at every point, called `up` and `down`. Their respective coordinates are denoted `(unx,uny,unz)` and `(dnx,dny,dnz)` and by plotting those vectors in an arrow plot, it is possible to check which side is `up` and which is `down`. In our case, the `up` side is the one outside the NP, hence the use of `up(emw.normE)` to specify the field norm outside.

A.3 Setting up the Perfectly Matched Layers

As the computational domain has to be meshed, a bounding box yielding appropriate physical conditions needs to be defined. The nature of the bounding box then depends on the problem at stake. Periodic boundary conditions will for example be chosen to simulate an array of particles. In the present case of an isolated particle, the bounding box has to be designed so as to prevent any reflection of the incident or scattered waves. One of the most efficient approach to achieve this is to set the bounding box as perfectly matched layers (PML). COMSOL provides ready-to-use PML settings, leaving the user to simply choose the most appropriate PML geometry for his problem, which is usually straightforward, though it remains the user's responsibility to ensure an adequate meshing of this region, meaning that a sufficient number of mesh elements is present across the thickness of the PML. Failing to do so will result in an inefficient PML and lead to an inaccurate

solution. For typical PML thicknesses of a fraction of the incident wavelength, the default meshing typically results in mesh nodes present only on the surfaces enclosing the PML. In other words, the PML region would only consist of a single mesh layer. To avoid this and refine the meshing, it is necessary to use a swept mesh across the PML domain, where the number of elements can be specified explicitly.

Note that for a cubical ("cartesian") PML region, one should make sure to mesh the cube faces using "mapped surfaces." All the internal surfaces of the cube have then to be converted into triangles in order to match the tetrahedral meshing of the volume.

The rest of the geometry can be meshed using standard methods, where triangles and tetrahedrons are used to mesh the surfaces and the volumes. The size of the meshing can be adjusted either with predefined COMSOL settings (...coarse, fine, finer,...) or with custom settings. Different elements in the geometry can be meshed with different precision by adding a "size" node to the considered element. See the provided example file for further details.

A.4 Far-Field Computations

We are interested in retrieving the optical far-field properties, such as the radiation profile or scattering matrix, of the particle under study. The size of the bounding box and our computing resources (and time) being finite, we have to resort to other solutions than just evaluating the fields "far" from the NP. A common approach for such problems is the use of near-field to far-field transformations, where the far-field amplitudes are obtained typically from integrals of near-field quantities. For scattering by a particle, the most common approach is based on the Stratton-Chu formula [27], where the far-field is obtained as an integral over the particle surface. In COMSOL 5.3, a "far-field" module has been implemented based on this approach. We summarize this method below to clarify the notations and conventions of far-field calculations in COMSOL.

The basic idea is that the knowledge of the EM field at the surface of the NP is able to provide the EM field anywhere else, explicitly (see [28] or Eq. 5.168 in [11]):

$$\mathbf{E}_{\text{sca}}(\mathbf{r}) = \iint_{\text{NP}} dS' \left\{ -i\omega\mu_0 [\mathbf{n}\times\mathbf{H}(\mathbf{r}')] \cdot \overleftrightarrow{G}(\mathbf{r},\mathbf{r}') + [\mathbf{n}\times\mathbf{E}(\mathbf{r}')] \cdot \left[\nabla \times \overleftrightarrow{G}(\mathbf{r},\mathbf{r}')\right] \right\} \quad (1)$$

where $\overleftrightarrow{G}(\mathbf{r},\mathbf{r}')$ is dyadic Green's function in the surrounding medium:

$$\overleftrightarrow{G}(\mathbf{r},\mathbf{r}') = \left(\overleftrightarrow{I} + \frac{1}{k_1^2}\nabla\otimes\nabla \right) g(\mathbf{r},\mathbf{r}') \quad (2)$$

with

$$g(\mathbf{r},\mathbf{r}') = \frac{e^{-ik_1|\mathbf{r}-\mathbf{r}'|}}{4\pi|\mathbf{r}-\mathbf{r}'|}$$

the scalar Green's function, $\overleftrightarrow{I}$ the identity dyadic, and $k_1 = k_0\sqrt{\epsilon_1}$ the wavenumber in the medium. Note that all those expressions are written here using the $\exp(+i\omega t)$ convention used by COMSOL.

Following [28], we define the induced electric $\mathbf{p} \equiv \mathbf{n}\times\mathbf{H}$ and magnetic $\mathbf{m} \equiv \mathbf{n}\times\mathbf{E}$ dipole moments.

As we are interested in the far-field (FF) ($r \longrightarrow \infty$, $\mathbf{E}(\mathbf{r})$ and $\mathbf{H}(\mathbf{r})$ perpendicular to $\mathbf{r}$), the following approximations can be made [28]:

$$\mathbf{p}\cdot\overleftrightarrow{G}(\mathbf{r},\mathbf{r}') \overset{\text{FF}}{\backsimeq} \frac{e^{-ik_1R}}{4\pi R}\left[\mathbf{p} - (\mathbf{p}\cdot\mathbf{e}_r)\mathbf{e}_r\right], \quad (3)$$

$$\mathbf{m}\cdot\left[\nabla\times\overleftrightarrow{G}(\mathbf{r},\mathbf{r}')\right] \overset{\text{FF}}{\backsimeq} -ik_1\frac{e^{-ik_1R}}{4\pi R}[\mathbf{e}_\mathbf{r}\times\mathbf{m}], \quad (4)$$

$$\frac{e^{-ik_1R}}{R} \overset{\text{FF}}{\backsimeq} \frac{e^{-ik_1r}}{r}e^{ik_1\mathbf{e}_\mathbf{r}\cdot\mathbf{r}'}, \quad \mathbf{e}_\mathbf{r} = \frac{\mathbf{r}}{r}. \quad (5)$$

where $R = |\mathbf{r}-\mathbf{r}'|$.

These approximations justify writing the scattered field in the far-field region as:

$$\mathbf{E}_{\text{sca}}(\mathbf{r}) \overset{\text{FF}}{\backsimeq} \frac{e^{-ik_1r}}{r}\left(E^\theta_{\text{far}}(\theta,\varphi)\mathbf{e}_\theta + E^\varphi_{\text{far}}(\theta,\varphi)\mathbf{e}_\varphi\right). \quad (6)$$

This expression defines the far-field amplitudes E^θ_{far} and E^φ_{far} as they are defined in COMSOL, but we note that different conventions may be used for this definition. We also note that within this definition, the far-field amplitudes have the dimension of electric field times length. We can also write the far-field components as:

$$E^\theta_{\text{far}} = \frac{-i}{4\pi}\iint_{\text{NP}} dS'\left[\omega\mu_0 p_\theta - k_1 m_\varphi\right]e^{ik_1\mathbf{e}_r\cdot\mathbf{r}'}$$

$$E^\varphi_{\text{far}} = \frac{-i}{4\pi}\iint_{\text{NP}} dS'\left[\omega\mu_0 p_\varphi + k_1 m_\theta\right]e^{ik_1\mathbf{e}_r\cdot\mathbf{r}'}$$

or equivalently as

$$E^\theta_{\text{far}} = \frac{-ik_1}{4\pi}\iint_{\text{NP}} dS'\left[Z_1 p_\theta - m_\varphi\right]e^{ik_1\mathbf{e}_r\cdot\mathbf{r}'}$$

$$E^\varphi_{\text{far}} = \frac{-ik_1}{4\pi}\iint_{\text{NP}} dS'\left[Z_1 p_\varphi + m_\theta\right]e^{ik_1\mathbf{e}_r\cdot\mathbf{r}'} \quad (7)$$

where $Z_1 = Z_0/\sqrt{\epsilon_1}$ has been defined earlier.

The far-field module in COMSOL provides a ready-made implementation of those formulae. It is necessary to add a "far-field domain" node in the "emw" node, which automatically adds a far-field option in the "post-processing" node of COMSOL. This simplifies the output of variables that are defined on the unit sphere (i.e., only

depend on θ and φ). Variables for the far-field amplitudes defined above can then be computed and plotted.

The SPlaC implementation [8, 33] of Mie theory provides the elements $S_1(\theta)$ and $S_2(\theta)$ of the scattering amplitude matrix with the same definitions and conventions as in Ref. [43]:

$$\mathbf{E}_{\mathrm{sca}}(\mathbf{r}) \overset{\mathrm{FF}}{\simeq} \frac{e^{ik_1 r}}{-ik_1 r} E_0 \left[\cos\varphi S_2(\theta)\mathbf{e}_\theta + \sin\varphi S_1(\theta)\mathbf{e}_\varphi\right]. \quad (8)$$

Taking into account the different convention for time-dependence ($\exp(-i\omega t)$), we therefore have the following equivalence between this formulation and the one of COMSOL summarized above:

$$E^{\theta}_{\mathrm{far}}(\theta, \phi = 0) \equiv S_2(\theta)^*/(ik_1) \quad (9)$$

$$E^{\phi}_{\mathrm{far}}(\theta, \phi = \pi/2) \equiv -S_1(\theta)^*/(ik_1) \quad (10)$$

These formulae were used to test the results of FEM far-field computations against Mie theory.

References

1. Draine BT, Flatau PJ (1994) Discrete-dipole approximation for scattering calculations. J Opt Soc Am A 11:1491–1499. https://doi.org/10.1364/JOSAA.11.001491
2. Mishchenko M, Hovenier J, Travis L (1999) Light scattering by nonspherical particles: theory, measurements, and applications. Academic Press, Cambridge
3. Parsons J, Burrows C, Sambles J, Barnes W (2010) A comparison of techniques used to simulate the scattering of electromagnetic radiation by metallic nanostructures. J Mod Opt 57:356–365. https://doi.org/10.1080/09500341003628702
4. Yurkin M (2013) Computational approaches for Plasmonics. In: D'Agostino S (ed) Handbook of molecular plasmonics. Pan Stanford Publishing, pp 83–135. https://doi.org/10.1201/b15328-4. http://www.crcnetbase.com/doi/abs/10.1201/b15328-4
5. Mishchenko MI, Lacis AA, Carlson BE, Travis LD (1995) Nonsphericity of dust-like tropospheric aerosols: implications for aerosol remote sensing and climate modeling. Geophys Res Lett 22:1077–1080. https://doi.org/10.1029/95GL00798
6. Draine BT (2003) Scattering by interstellar dust grains. I. Optical and ultraviolet. Astrophys J 598:1017
7. Le Ru EC, Etchegoin PG, Meyer M (2006) Enhancement factor distribution around a single surface-enhanced Raman scattering hot spot and its relation to single molecule detection. J Chem Phys 125(20):204701
8. Le Ru EC, Etchegoin PG (2009) Principles of surface-enhanced Raman spectroscopy and related plasmonic effects. Elsevier, Amsterdam
9. Nieminen TA, Loke VLY, Stilgoe AB, Knöner G, Brańczyk AM, Heckenberg NR, Rubinsztein-Dunlop H (2007) Optical tweezers computational toolbox. J Optics A: Pure and Applied Optics 9:S196
10. Bohren CF, Huffman DR (1983) Absorption and scattering of light by small particles. Wiley, New York
11. Mishchenko MI, Travis LD, Lacis AA (2002) Scattering, absorption and emission of light by small particles, 3rd electronic release edn. Cambridge University Press, Cambridge
12. Taflove A, Hagness S (2000) Computational electrodynamics: the finite-difference time-domain method. Artech House, Boston
13. Jin J (2002) The finite element method in electromagnetics, 2nd. Wiley-IEEE Press, New York
14. Monk P (2003) Finite element method for Maxwell's equations. Clarendon Press, Oxford
15. Berenger JP (1994) A perfectly matched layer for the absorption of electromagnetic waves. J Comput Phys 114:185–200
16. Hoffmann J, Hafnera C, Leidenbergera P, Hesselbartha J, Burgerb S (2009) Comparison of electromagnetic field solvers for the 3D analysis of plasmonic nano antennas. https://doi.org/10.1117/12.828036
17. Khoury CG, Norton SJ, Vo-Dinh T (2010) Investigating the plasmonics of a dipole-excited silver nanoshell: Mie theory versus finite element method. Nanotechnology 21:315203
18. Khoury CG, Norton SJ, Vo-Dinh T (2009) Plasmonics of 3-D nanoshell dimers using multipole expansion and finite element method. ACS Nano 3:2776–2788. https://doi.org/10.1021/nn900664j
19. Karamehmedović M, Schuh R, Schmidt V, Wriedt T, Matyssek C, Hergert W, Stalmashonak A, Seifert G, Stranik O (2011) Comparison of numerical methods in near-field computation for metallic nanoparticles. Opt Express 19(9):8939–8953. https://doi.org/10.1364/OE.19.008939
20. Loke VLY, Huda GM, Donev EU, Schmidt V, Hastings JT, Mengüç MP, Wriedt T (2014) Comparison between discrete dipole approximation and other modelling methods for the plasmonic response of gold nanospheres. Appl Phys B 115(2):237–246. https://doi.org/10.1007/s00340-013-5594-z
21. Mezghani F, Barchiesi D, Cherouat A, Grosges T, Borouchaki H (2015) Comparison of 3D adaptive remeshing strategies for finite element simulations of electromagnetic heating of gold nanoparticles. Adv Math Phys 2015:469310
22. Yang J, Hugonin JP, Lalanne P (2016) Near-to-far field transformations for radiative and guided waves. ACS Photonics 3:395–402. https://doi.org/10.1021/acsphotonics.5b00559
23. Kupresak M, Zheng X, Vandenbosch GAE, Moshchalkov VV (2017) Benchmarking of software tools for the characterization of nanoparticles. Opt Express 25(22):26760–26780. https://doi.org/10.1364/OE.25.026760
24. Somerville WRC, Auguié B, Le Ru EC (2015) Accurate and convergent T-matrix calculations of light scattering by spheroids. J Quant Spectrosc Rad Transf 160:29–35
25. Gérardy JM, Ausloos M (1982) Absorption spectrum of clusters of spheres from the general solution of Maxwell's equations. II. Optical properties of aggregated metal spheres. Phys Rev B 25(6):4204–4229
26. Allardice JR, Le Ru EC (2014) Convergence of Mie theory series: criteria for far-field and near-field properties. Appl Optics 53:7224–7229
27. Stratton JA, Chu LJ (1939) Diffraction theory of electromagnetic waves. Phys Rev 56:99–107. https://doi.org/10.1103/PhysRev.56.99
28. Auguié B, Somerville WRC, Roache S, Le Ru EC (2016) Numerical investigation of the Rayleigh hypothesis for electromagnetic scattering by a particle. J Opt 18:075007
29. Haiss W, Thanh NTK, Aveyard J, Fernig DG (2007) Determination of size and concentration of gold nanoparticles from UV-vis spectra. Anal Chem 79(11):4215–4221. https://doi.org/10.1021/ac0702084
30. Huang X, Jain PK, El-Sayed IH, El-Sayed MA (2007) Plasmonic photothermal therapy (PPTT) using gold nanoparticles. Lasers Med. Sci. 23(3):217. https://doi.org/10.1007/s10103-007-0470-x
31. Darby BL, Auguié B, Meyer M, Pantoja AE, Le Ru EC (2016) Modified optical absorption of molecules on metallic nanoparticles at sub-monolayer coverage. Nat Photon 10:40–45

32. Etchegoin PG, Le Ru EC, Meyer M (2006) An analytic model for the optical properties of gold. J Chem Phys 125:164705. https://doi.org/10.1063/1.2360270
33. Le Ru EC, Etchegoin PG SERS and plasmonics codes (SPlaC). Matlab codes freely available from http://www.vuw.ac.nz/raman/book/codes.aspx
34. Aslan K, Leonenko Z, Lakowicz JR, Geddes CD (2005) Fast and slow deposition of silver nanorods on planar surfaces: application to metal-enhanced fluorescence. J Phys Chem B 109(8):3157–3162. https://doi.org/10.1021/jp045186t
35. Schmucker AL, Harris N, Banholzer MJ, Blaber MG, Osberg KD, Schatz GC, Mirkin CA (2010) Correlating nanorod structure with experimentally measured and theoretically predicted surface plasmon resonance. ACS Nano 4(9):5453–5463. https://doi.org/10.1021/nn101493t
36. Le Ru EC, Grand J, Sow I, Somerville WRC, Etchegoin PG, Treguer-Delapierre M, Charron G, Felidj N, Levi G, Aubard J (2011) A scheme for detecting every single target molecule with surface-enhanced Raman spectroscopy. Nano Lett 11:5013
37. Gill R, Le Ru EC (2011) Fluorescence enhancement at hot-spots: The case of Ag nanoparticle aggregates. Phys Chem Chem Phys 13:16366–16372
38. Le Ru EC, Etchegoin PG (2012) Single molecule surfaced-enhanced Raman spectroscopy. Annu Rev Phys Chem 63:65–87
39. Thacker VV, Herrmann LO, Sigle DO, Zhang T, Liedl T, Baumberg JJ, Keyser UF (2014) DNA origami based assembly of gold nanoparticle dimers for surface-enhanced Raman scattering. Nat Commun 5:3448. https://doi.org/10.1038/ncomms4448
40. Somerville WRC, Auguié B, Le Ru EC (2012) Severe loss of precision in calculations of T-matrix integrals. J Quant Spectrosc Rad Transf 113(7):524–535
41. Somerville WRC, Auguié B, Le Ru EC (2013) A new numerically stable implementation of the T-matrix method for electromagnetic scattering by spheroidal particles. J Quant Spectrosc Rad Transf 123:153–168
42. Somerville WRC, Auguié B, Le Ru EC (2016) SMARTIES: user-friendly codes for fast and accurate calculations of light scattering by spheroids. J Quant Spectrosc Rad Transf 174:39–55
43. Bohren CF, Huffman DR (1983) Absorption and scattering of light by small particles. Wiley, New York

60nm Gold Sphere in eps=4 medium

Contents

1. Global Definitions

GLOBAL SETTINGS

COMSOL version	COMSOL 5.3 (Build: 223)
Unit system	SI

1.1. PARAMETERS 1

PARAMETERS

Name	Expression	Value	Description
E0	1[V/m]	1 V/m	
eps_ext	4	4	
lambda	650	650	
lambda_min	500	500	for lambda sweep
lambda_max	800	800	for lambda sweep
lambda_step	5	5	for lambda sweep
t_pml	100	100	PML Thickness
radius	30	30	NP radius
S0	E0^2/(2*Z1)	0.0026544 W/m^2	
r_pml	350	350	PML radius
Z1	Z0_const/sqrt(eps_ext)	188.37 Ω	
nblayer_pml	5	5	

2. Component

COMPONENT SETTINGS

Unit system	SI
Geometry shape order	automatic

2.1. DEFINITIONS

2.1.1. Variables

Variables

SELECTION

Geometric entity level	Entire model

Name	Expression	Unit	Description
k1	emw.k0*sqrt(eps_ext)	rad/m	Incident wavevector
sigma_geom	int_surf(1)	m^2	NP area
nrelPoav	nx*up(emw.relPoavx) + ny*up(emw.relPoavy) + nz*up(emw.relPoavz)	W/m^2	Poynting vector
sigma_sc	int_surf(nrelPoav)/S0	m^2	Scattering cross-section
sigma_abs	int_vol(emw.Qh)/S0	m^2	Absorption cross-section
sigma_ext	sigma_sc + sigma_abs	m^2	Extinction cross-section
sigma_extOT	-4*pi/(emw.k0*sqrt(eps_ext))*int_OT(imag(emw.Efarx*1[m]))/E0	m^2	Optical Theorem
M_ave	int_surf((up(emw.normE))^2)/sigma_geom/E0^2		Average EF

2.1.2. Component Couplings

Int_vol

Coupling type	Integration
Operator name	int_vol

SOURCE SELECTION

Geometric entity level	Domain
Name	Nanoparticle
Selection	Domain 6

Int_surf

Coupling type	Integration
Operator name	int_surf

SOURCE SELECTION

Geometric entity level	Boundary
Name	Nanoparticle surface
Selection	Boundaries 13–16, 24–25, 30–31

Int_optical Theorem

Coupling type	Integration
Operator name	int_OT

SOURCE SELECTION

Geometric entity level	Point
Selection	Point 10

2.1.3. Selections

Physical Domains

Selection type
Explicit

Selection
Domains 5–6

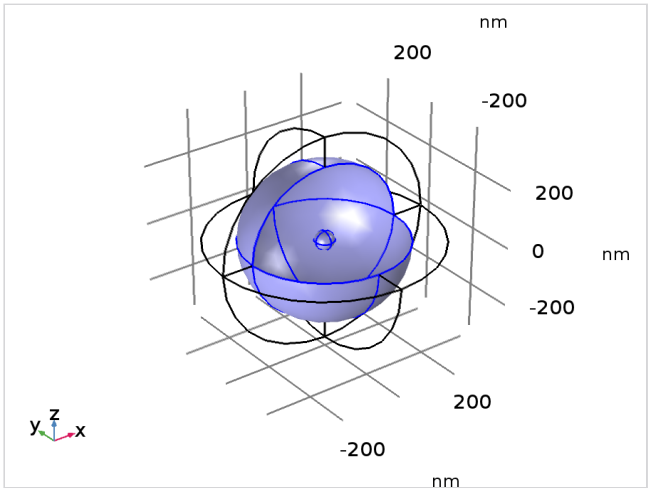

Physical domains

Nanoparticle

Selection type
Explicit

Selection
Domain 6

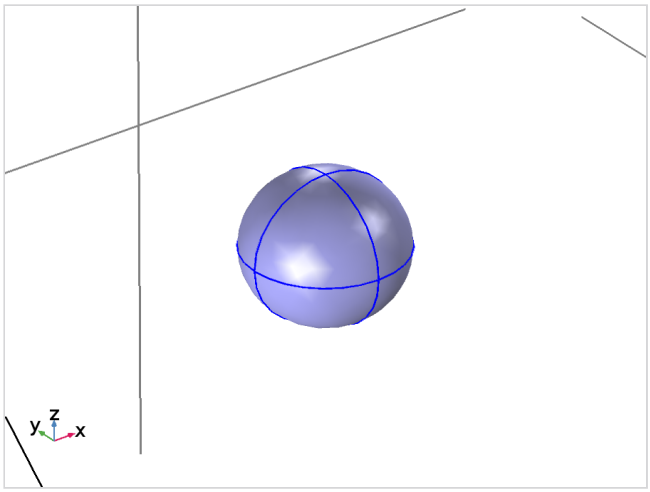

Nanoparticle

Nanoparticle Surface

Selection type
Explicit

Selection
Boundaries 13–16, 24–25, 30–31

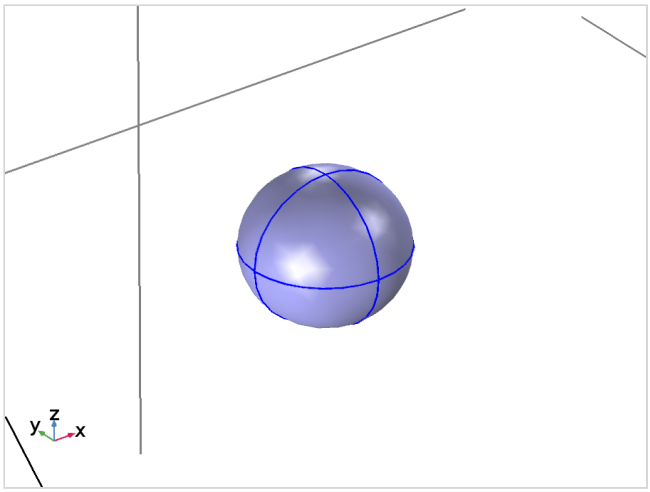

Nanoparticle surface

PML

Selection type
Complement

Selection
Domains 1–4, 7–10

GEOMETRIC ENTITY LEVEL

Description	Value
Level	Domain

INPUT ENTITIES

Description	Value
Selections to invert	Physical domains

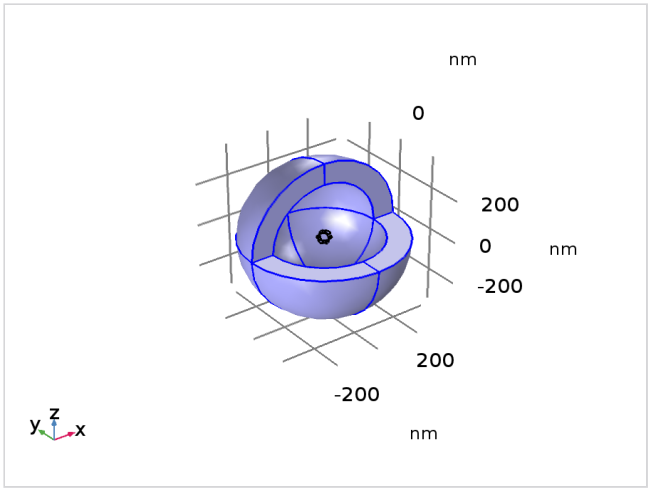

PML

2.1.4. Coordinate Systems

Boundary System 1

Coordinate system type	Boundary system
Tag	sys1

2.1.5. Domain Properties

Perfectly Matched Layer

Tag	pml1

SELECTION

Geometric entity level	Domain
Name	PML
Selection	Domains 1–4, 7–10

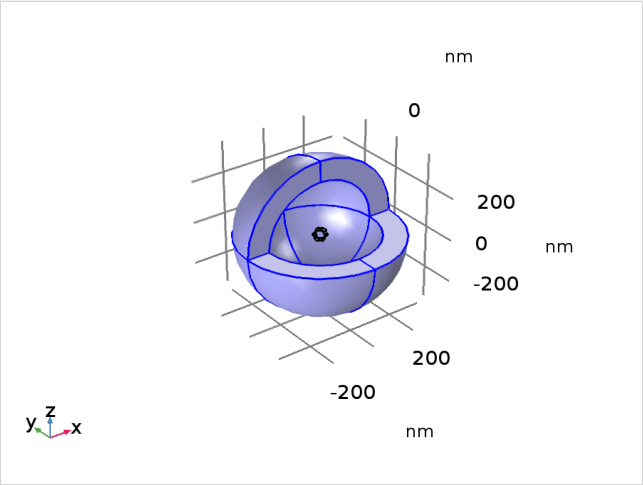

Selection

GEOMETRY

Description	Value
Coordinate names	{x, y, z}
Type	Spherical

NULL

x (m)	y (m)	z (m)
0	0	0

SCALING

Description	Value
Coordinate stretching type	Polynomial

SETTINGS

Description	Value
Typical wavelength from	Physics interface
Physics	Electromagnetic Waves, Frequency Domain
PML scaling factor	0.5

2.2. GEOMETRY

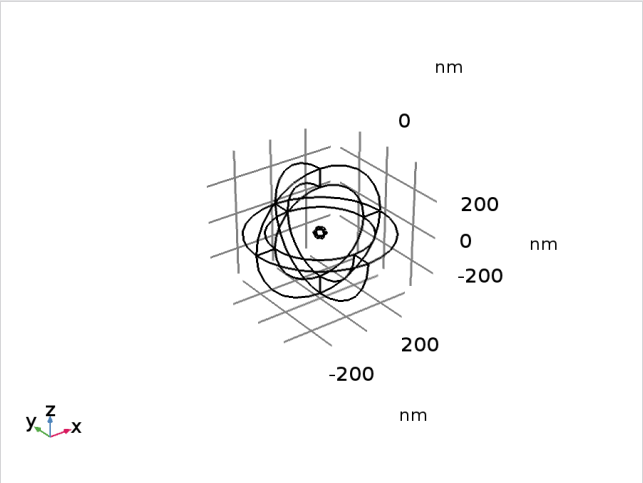

Geometry

UNITS

Length unit	nm
Angular unit	deg

GEOMETRY STATISTICS

Description	Value
Space dimension	3
Number of domains	10
Number of boundaries	36
Number of edges	42
Number of vertices	18

2.2.1. Sphere (Sph1)

POSITION

Description	Value
Position	{0, 0, 0}

AXIS

Description	Value
Axis type	z - axis

SIZE

Description	Value
Radius	radius

2.2.2. Sphere 2 (Sph2)

POSITION

Description	Value
Position	{0, 0, 0}

AXIS

Description	Value
Axis type	z - axis

AXIS

Layer name	Thickness (nm)
Layer 1	t_pml

SIZE

Description	Value
Radius	r_pml

2.3. MATERIALS

2.3.1. Ext

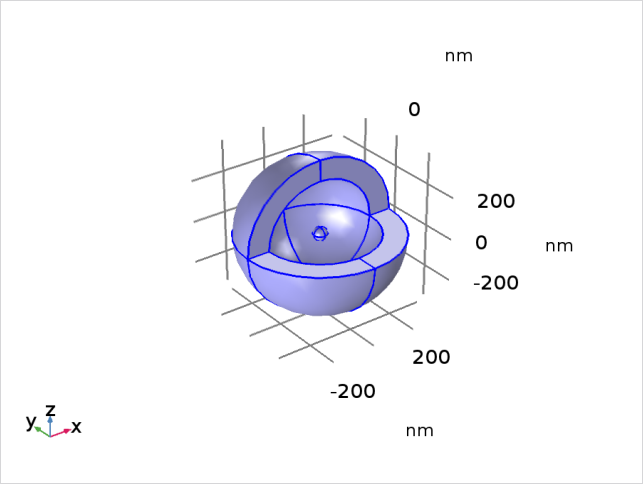

ext

SELECTION

Geometric entity level	Domain
Selection	Domains 1–5, 7–10

MATERIAL PARAMETERS

Name	Value	Unit
Relative permittivity	eps_ext	1
Relative permeability	1	1
Electrical conductivity	0	S/m

2.3.2. Gold

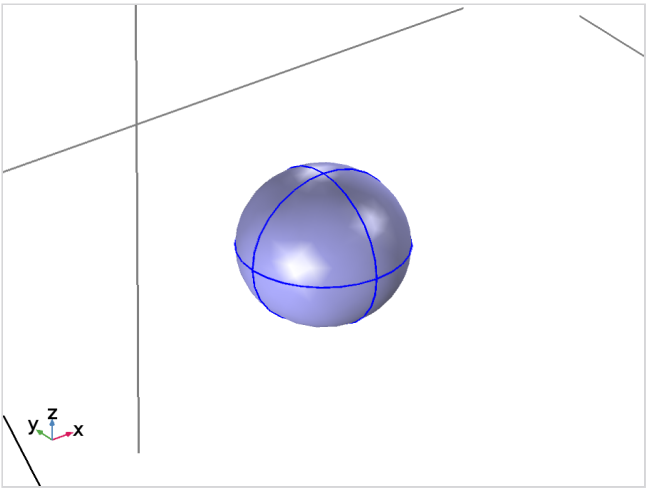

gold

SELECTION

Geometric entity level	Domain
Selection	Domain 6

MATERIAL PARAMETERS

Name	Value	Unit
Relative permittivity	conj(1.54*(1-1/(177.5^2*((1/lambda)^2+i/(14500*lambda))))+1.27/470*(exp(i*(-pi/4))/(1/470-1/lambda-i/1900)+exp(-i*(-pi/4))/(1/470+1/lambda+i/1900))+1.1/325*(exp(i*(-pi/4))/(1/325-1/lambda-i/1060)+exp(-i*(-pi/4))/(1/325+1/lambda+i/1060)))	1
Relative permeability	1	1
Electrical conductivity	0	S/m

2.4. ELECTROMAGNETIC WAVES, FREQUENCY DOMAIN

SELECTION

Geometric entity level	Domain
Selection	Domains 1–10

EQUATIONS

$$\nabla \times \mu_r^{-1}(\nabla \times \mathbf{E}) - k_0^2(\epsilon_r - \frac{j\sigma}{\omega\epsilon_0})\mathbf{E} = \mathbf{0}$$

SETTINGS

Description	Value
Electric field	Quadratic
Value type when using splitting of complex variables	Complex
Formulation	Scattered field
Background wave type	User defined
Background electric field, x component	E0*exp(-i*k1*z)
Background electric field, y component	0
Background electric field, z component	0
Activate port sweep	Off
Enable	Off
Methodology options	Robust

2.4.1. Wave Equation, Electric 1

SELECTION

Geometric entity level	Domain
Selection	Domains 1–10

EQUATIONS

$$\nabla \times \mu_r^{-1}(\nabla \times \mathbf{E}) - k_0^2(\epsilon_r - \frac{j\sigma}{\omega\epsilon_0})\mathbf{E} = \mathbf{0}$$

SETTINGS

Description	Value
Electric displacement field model	Relative permittivity
Relative permittivity	From material
Constitutive relation	Relative permeability
Relative permeability	From material
Electrical conductivity	From material

PROPERTIES FROM MATERIAL

Property	Material	Property group

Relative permittivity	ext	Basic
Relative permeability	ext	Basic
Electrical conductivity	ext	Basic
Relative permittivity	gold	Basic
Relative permeability	gold	Basic
Electrical conductivity	gold	Basic

2.4.2. Perfect Electric Conductor 1

SELECTION

Geometric entity level	Boundary
Selection	Boundaries 5–8, 20–21, 28, 35

EQUATIONS

$$\mathbf{n} \times \mathbf{E} = \mathbf{0}$$

SETTINGS

Description	Value
Apply reaction terms on	All physics (symmetric)
Use weak constraints	Off
Constraint method	Elemental

2.4.3. Initial Values 1

SELECTION

Geometric entity level	Domain
Selection	Domains 1–10

2.4.4. Far-Field Domain 1

SELECTION

Geometric entity level	Domain
Selection	Domain 5

Far-Field Calculation 1

SELECTION

Geometric entity level	Boundary
Name	Nanoparticle surface
Selection	Boundaries 13–16, 24–25, 30–31

SETTINGS

Description	Value
Far-field variable name	Efar
Symmetry in the x=0 plane	Off
Symmetry in the y=0 plane	Off
Symmetry in the z=0 plane	Off
Boundary relative to domain	Inside

2.5. MESH

MESH STATISTICS

Description	Value
Minimum element quality	0.1419

Average element quality	0.7439
Tetrahedral elements	79571
Prism elements	6540
Triangular elements	3468
Quadrilateral elements	600
Edge elements	366
Vertex elements	18

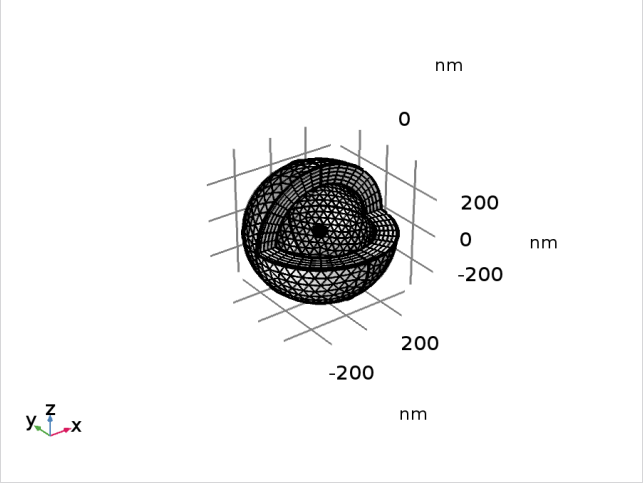

Mesh

2.5.1. Size (Size)

SETTINGS

Description	Value
Maximum element size	56
Minimum element size	7
Curvature factor	0.5
Resolution of narrow regions	0.6
Maximum element growth rate	1.45
Predefined size	Fine

2.5.2. Free Triangular 1 (Ftri1)

SELECTION

Geometric entity level	Boundary
Selection	Boundaries 5–8, 20–21, 28, 35

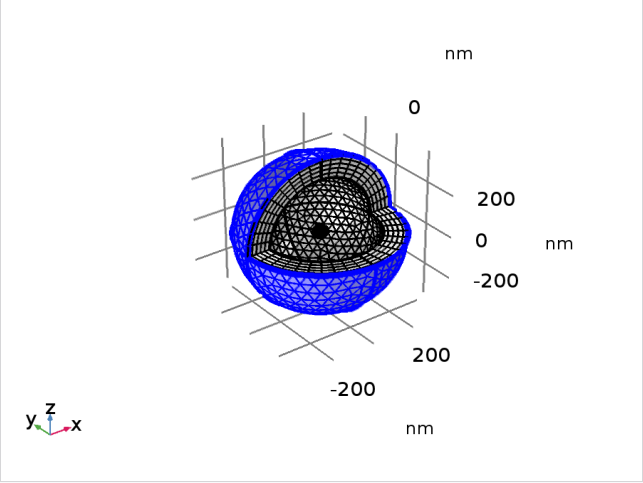

Free Triangular 1

2.5.3. Swept 1 (Swe1)

SELECTION

Geometric entity level	Domain
Name	PML
Selection	Domains 1–4, 7–10

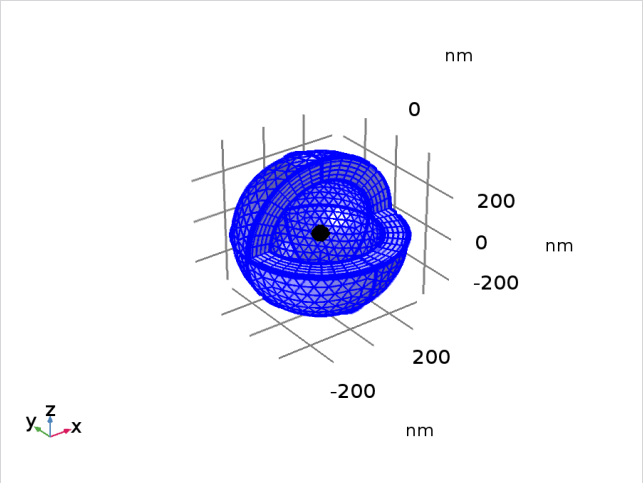

Swept 1

SETTINGS

Description	Value
Face meshing method	Quadrilateral (legacy version 5.2)

Distribution 1 (Dis1)

SELECTION

Geometric entity level	Domain
Selection	Domains 1–4, 7–10

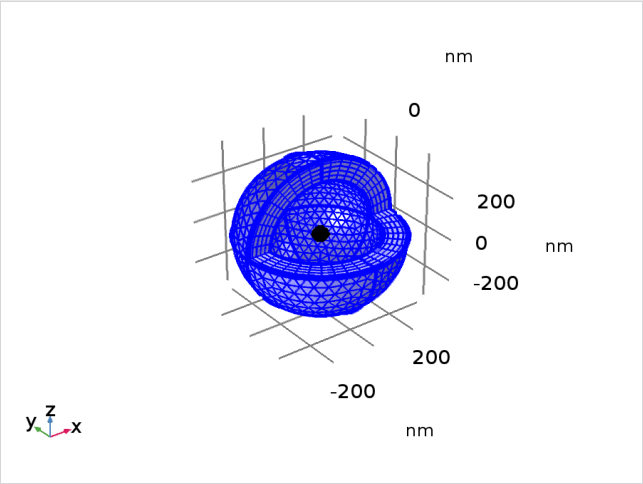

Distribution 1

SETTINGS

Description	Value
Number of elements	nblayer_pml

2.5.4. Free Triangular 2 (Ftri2)

SELECTION

Geometric entity level	Boundary
Name	Nanoparticle surface
Selection	Boundaries 13–16, 24–25, 30–31

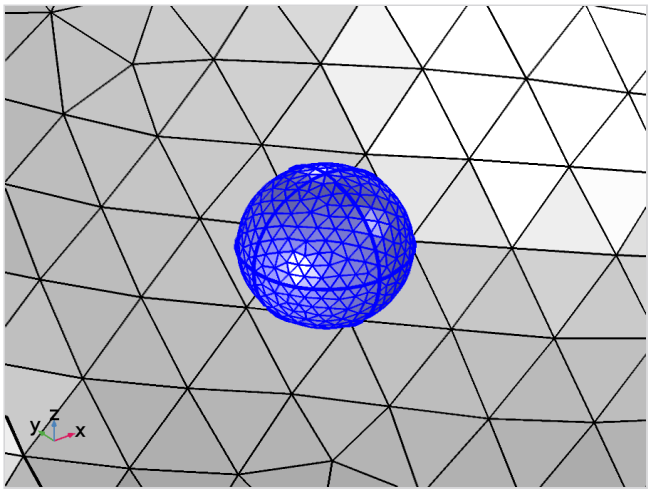

Free Triangular 2

Size 1 (Size1)

SELECTION

Geometric entity level	Domain
Name	Nanoparticle
Selection	Domain 6

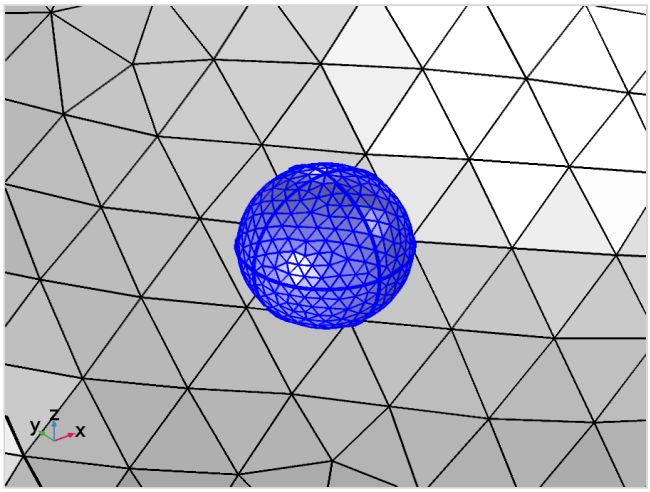

Size 1

SETTINGS

Description	**Value**
Maximum element size	14
Minimum element size	0.14
Curvature factor	0.2
Maximum element growth rate	1.3
Predefined size	Extremely fine

2.5.5. Free Tetrahedral 1 (Ftet1)

SELECTION

Geometric entity level	Domain

Selection	Remaining

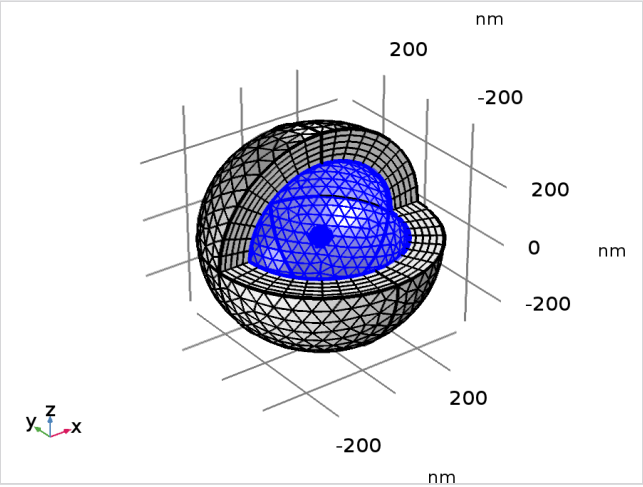

Free Tetrahedral 1

SETTINGS

Description	Value
Method	Delaunay (legacy version)

Size 1 (Size1)

SELECTION

Geometric entity level	Domain
Selection	Geometry geom1

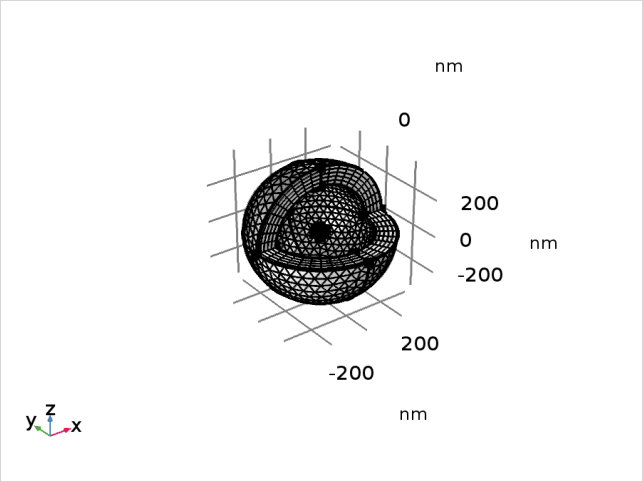

Size 1

SETTINGS

Description	Value
Maximum element size	24.5
Minimum element size	1.05
Curvature factor	0.3
Resolution of narrow regions	0.85
Maximum element growth rate	1.35
Predefined size	Extra fine

3. Study

COMPUTATION INFORMATION

Computation time	1 min 16 s
CPU	Intel(R) Core(TM) i7-5500U CPU @ 2.40GHz, 2 cores
Operating system	Windows 10

3.1. FREQUENCY DOMAIN

Frequencies (Hz)
c_const/lambda[nm]

STUDY SETTINGS

Description	**Value**
Include geometric nonlinearity	Off

PHYSICS AND VARIABLES SELECTION

Physics interface	**Discretization**
Electromagnetic Waves, Frequency Domain (emw)	physics

MESH SELECTION

Geometry	**Mesh**
Geometry (geom1)	mesh1

3.2. SOLVER CONFIGURATIONS

3.2.1. Solution 1

Compile Equations: Frequency Domain (St1)

STUDY AND STEP

Description	**Value**
Use study	Study
Use study step	Frequency Domain

Dependent Variables 1 (V1)

GENERAL

Description	**Value**
Defined by study step	Frequency Domain

INITIAL VALUE CALCULATION CONSTANTS

Description	**Value**
Parameter initial value list	c_const/lambda[nm]

Electric Field (Comp1.E) (Comp1_E)

GENERAL

Description	**Value**
Field components	{comp1.Ex, comp1.Ey, comp1.Ez}

Stationary Solver 1 (S1)

GENERAL

Description	**Value**
Defined by study step	Frequency Domain

Advanced (ADef)

ASSEMBLY SETTINGS

Description	**Value**

Allow complex-valued output from functions with real input	On

Parametric 1 (P1)

GENERAL

Description	Value
Defined by study step	Frequency Domain
Parameter value list	c_const/lambda[nm]
Run continuation for	No parameter

Fully Coupled 1 (Fc1)

GENERAL

Description	Value
Linear solver	Iterative 1

Iterative 1 (I1)

GENERAL

Description	Value
Solver	BiCGStab

Multigrid 1 (Mg1)

GENERAL

Description	Value
Use hierarchy in geometries	Geometry

Presmoother (Pr)

SOR Vector 1 (Sv1)

MAIN

Description	Value
Variables	Electric field (comp1.E)

Postsmoother (Po)

SOR Vector 1 (Sv1)

MAIN

Description	Value
Variables	Electric field (comp1.E)

Coarse Solver (Cs)

Direct (DDef)

GENERAL

Description	Value
Out-of-core	Off

4. Results

4.1. DATA SETS

4.1.1. Study/Solution

SOLUTION

Description	Value
Solution	Solution 1
Component	Save Point Geometry 1

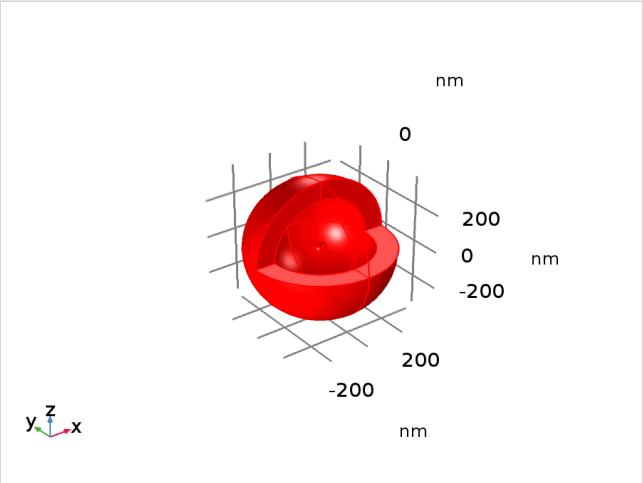

Data set: Study/Solution

4.1.2. CutLineAlongX

DATA

Description	Value
Data set	Study/Solution

PARAMETER

Description	Value
Minimum	-1
Maximum	1

EXPRESSIONS

Description	Value
x	r_pml*s
y	0
z	0

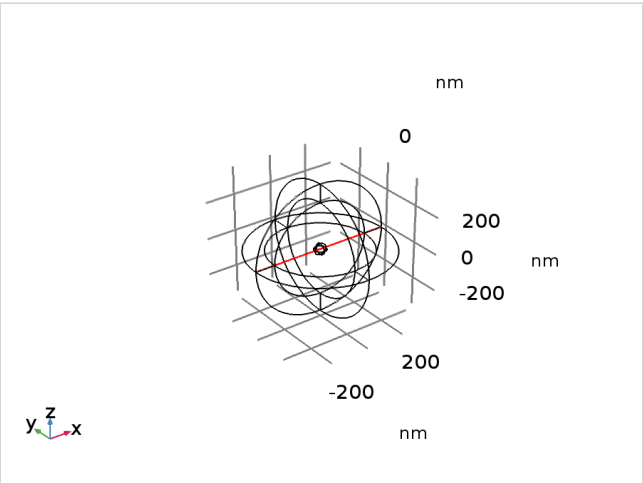

Data set: CutLineAlongX

4.1.3. CutLineSurface

DATA

Description	Value
Data set	Study/Solution

PARAMETER

Description	Value
Minimum	0
Maximum	pi

EXPRESSIONS

Description	Value
x	(radius + 0.0001)*sin(s)
y	0
z	(radius + 0.0001)*cos(s)

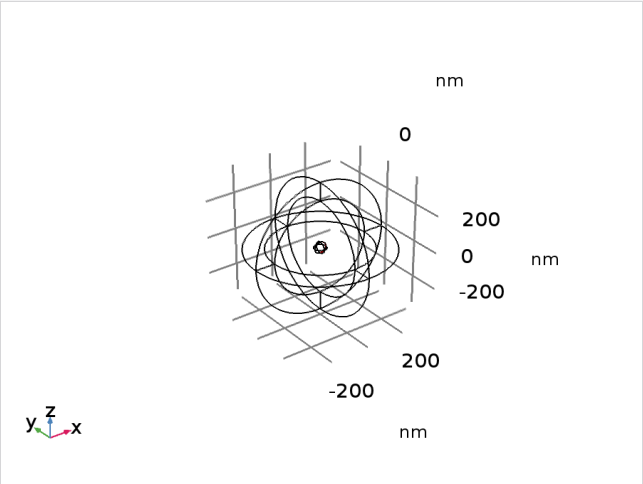

Data set: CutLineSurface

4.2. DERIVED VALUES

4.2.1. Global Evaluation

DATA

Description	Value
Data set	Study/Solution

EXPRESSIONS

Expression	Unit	Description
sigma_abs	m^2	Absorption cross-section
sigma_sc	m^2	Scattering cross-section
sigma_ext	m^2	Extinction cross-section
sigma_extOT	m^2	Optical Theorem
M_ave	1	Average EF

OUTPUT

Evaluated in	cross-sections and average EF

4.3. TABLES

4.3.1. Cross-Sections and Average EF

Global Evaluation (sigma_abs, sigma_sc, sigma_ext, sigma_extOT, M_ave)

CROSS-SECTIONS AND AVERAGE EF

freq (Hz)	Absorption cross-section (m^2)	Scattering cross-section (m^2)	Extinction cross-section (m^2)	Optical Theorem (m^2)	Average EF
4.6122E14	9.5367E-15	2.3452E-14	3.2989E-14	3.2989E-14	63.744

4.4. PLOT GROUPS

4.4.1. Electric Field (Emw)

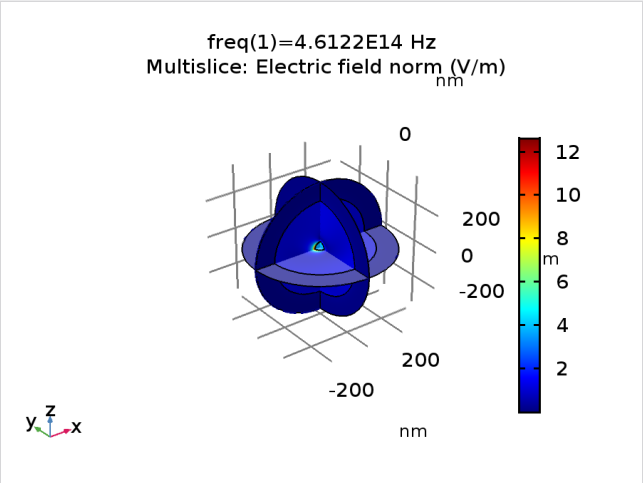

freq(1)=4.6122E14 Hz Multislice: Electric field norm (V/m)

4.4.2. FarField S2 (XOz)

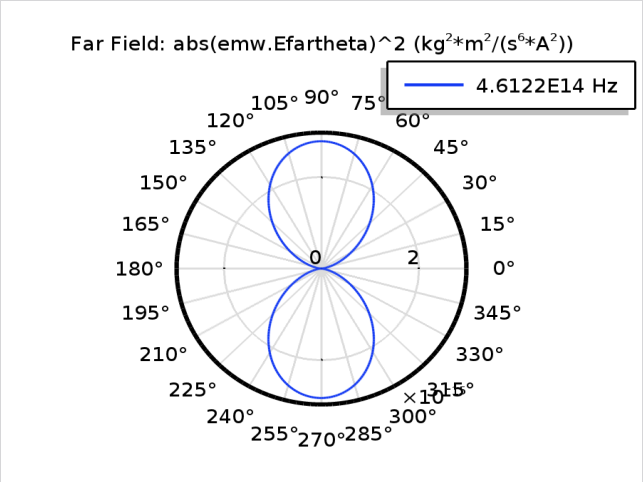

*Far Field: abs(emw.Efartheta)^2 (kg²*m²/(s⁶*A²))*

4.4.3. Far Field S1 (YOz)

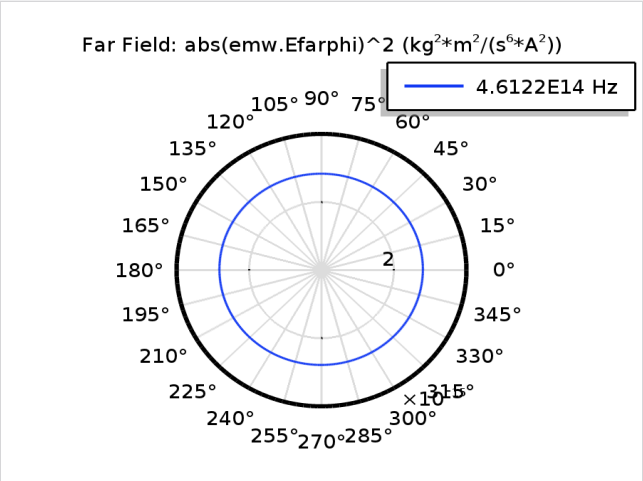

*Far Field: abs(emw.Efarphi)^2 (kg²*m²/(s⁶*A²))*

4.4.4. Plot M(X)

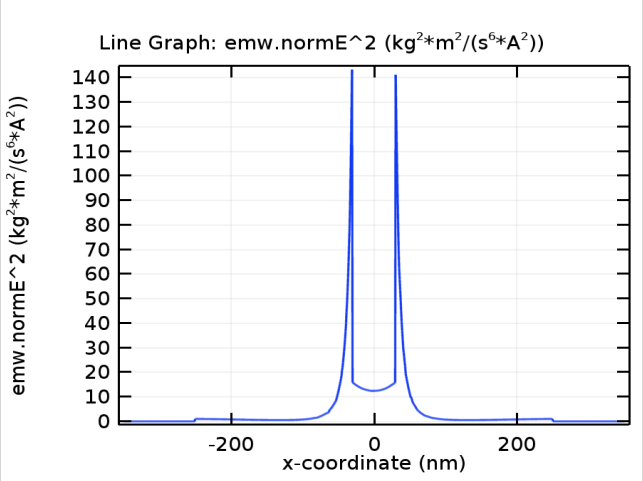

Line Graph: emw.normE^2 ($kg^2*m^2/(s^6*A^2)$)

4.4.5. Plot Msurf(Theta)

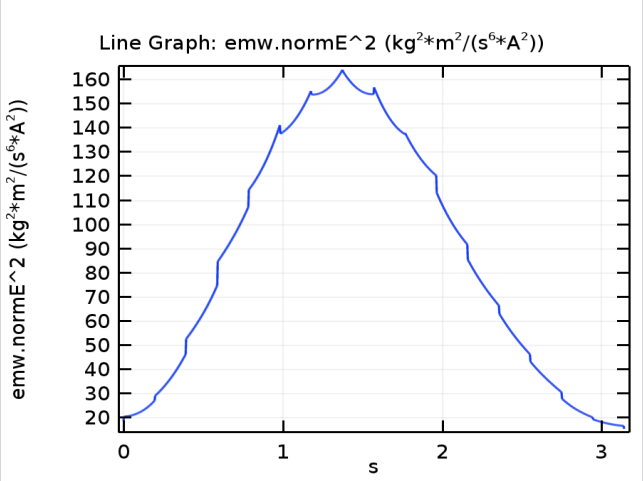

Line Graph: emw.normE^2 ($kg^2*m^2/(s^6*A^2)$)